Title:

Targeting mechanistic target of rapamycin complex 2 attenuates immunopathology in Systemic Lupus Erythematosus

Authors:

Minji Ai B.Sc., MRes, Ph.D.[1], Xian Zhou B.Sc., Ph.D.[1], Michele Carrer B.Sc., Ph.D.[2], Paymaan Jafar-nejad M.D. [2], Yanfeng Li B.Sc., Ph.D.[1], Naomi Gades D.V.M., M.S.[3], Mariam Alexander M.D.[4], Mario A. Bautista M.D.[1], Ali A. Duarte Garcia M.D.[1], Hu Zeng B.Sc., Ph.D.[1,5]

[1]Division of Rheumatology, Department of Medicine, Mayo Clinic Rochester, MN, USA
[2]Ionis Pharmaceuticals, Carlsbad, CA, USA
[3]Department of Comparative Medicine, Mayo Clinic Arizona, USA
[4]Division of Laboratory Medicine and Pathology, Mayo Clinic Rochester, MN, USA
[5]Department of Immunology, Mayo Clinic Rochester, MN, USA

Address correspondence to:

Hu Zeng, Ph.D.

Division of Rheumatology, Department of Medicine; Department of Immunology

Mayo Clinic Rochester, 200 First St SW, Rochester, MN 55905

Telephone: +1 (507) 266-5823; Fax: +1 (507) 284-1637;

E-mail: zeng.hu1@mayo.edu

Running title: Targeting mTORC2 benefits SLE

Grant support: This work is supported by NIH R01AR077518 and R01AI162678 (to H.Z.), lupus Research Alliance (696599, to H.Z.) and Mayo Foundation for Medical Education and Research.

Competing interests: Michele Carrer and Paymaan Jafar-nejad are paid employees of Ionis Pharmaceuticals.

Abstract

Objective: We aim to explore the role of mechanistic target of rapamycin complex (mTORC) 2 in systemic lupus erythematosus (SLE) development, the in *vivo* regulation of mTORC2 by type I interferon (IFN) signaling in autoimmunity, and to use mTORC2 targeting therapy to ameliorate lupus-like symptoms in an *in vivo* lupus mouse model and an *in vitro* coculture model using human PBMCs.

Method: We first induced lupus-like disease in T cell specific *Rictor*, a key component of mTORC2, deficient mice by topical application of imiquimod (IMQ) and monitored disease development. Next, we investigated the changes of mTORC2 signaling and immunological phenotypes in type I IFNAR deficient Lpr mice. We then tested the beneficial effects of anti-*Rictor* antisense oligonucleotide (*Rictor*-ASO) in a mouse model of lupus: MRL/*lpr* mice. Finally, we examined the beneficial effects of *RICTOR*-ASO on SLE patients' PBMCs using an *in vitro* T-B cell coculture assay.

Results: T cell specific *Rictor* deficient mice have reduced age-associated B cells, plasma cells and germinal center B cells, and less autoantibody production than WT mice following IMQ treatment. IFNAR1 deficient Lpr mice have reduced mTORC2 activity in $CD4^+$ T cells accompanied by restored $CD4^+$ T cell glucose metabolism, partially recovered T cell trafficking, and reduced systemic inflammation. *In vivo Rictor*-ASO treatment improves renal function and pathology in MRL/*lpr* mice, along with improved immunopathology. In human SLE (N = 5) PBMCs derived T-B coculture assay, *RICTOR*-ASO significantly reduce immunoglobulin and autoantibodies production ($P < 0.05$).

Conclusion: Targeting mTORC2 could be a promising therapeutic for SLE.

52 **Keywords**: Systemic lupus erythematosus, mTORC2, antisense oligonucleotide,

53 immunopathology

54

Introduction

Systemic lupus erythematosus (SLE) is an autoimmune disease characterized by loss of tolerance to self-antigen and the production of autoantibodies. An estimated of 0.40 million people are diagnosed with SLE annually among whom over 85% are young female patients globally (1). SLE is known for its heterogeneity. It presents various clinical manifestations, from mild skin rashes to life-threatening multi-organ damages such as nephritis, cerebritis, and myelofibrosis (2). Broad immunosuppressive agents such as azathioprine are commonly used for SLE management which may not lead to optimal disease control and can lead to undesired side effects (3). Unlike rheumatoid arthritis with numerous disease-specific biologics, only two biological agents, belimumab and anifrolumab, are approved for SLE treatment (4). Therefore, a better understanding of SLE pathogenesis is urgently needed for the development of novel and specific therapeutic agents.

SLE is a heterogeneous disease influenced by various factors including genetic, environmental, and immunological factors (5). Multiple molecular pathways, particularly type I interferon (IFN) signaling, have been proposed to play pivotal roles in disease pathogenesis (6). Over-activation of plasmacytoid dendritic cells (pDCs) leads to elevated IFNα and induced genes, the type I IFN signature, in SLE patients (7), which promote the presentation of self-antigens to autoreactive T and B cells leading to autoimmunity (8). Injection of IFN-αβ to NZB/W F1 mice has led to the rapid onset of lupus-like diseases (9). Conversely, IFN-I receptor-deficient mice were partially protected from pristane induced lupus mice (10), lupus-prone NZB mice (11) and C57BL/6-Fas^{lpr} mice (12) . Although one report indicated that deficiency of type II but not type I IFN receptor ameliorates lupus-like diseases in MRL/*lpr* mice (13), treatment with anti-IFNAR blocking

78 antibody alleviated lupus-like symptoms in MRL/*lpr* mice (14), suggesting a disease promoting
79 function of type I IFN in MRL/*lpr* model. Monoclonal antibodies directed at the type I IFN receptor,
80 such as Anifrolumab, have been actively tested in clinical trials for SLE treatment and showed
81 promising outcomes (15). Despite the well-known link between type I IFN signature and SLE,
82 there are several outstanding questions in this context, including the mechanisms through which
83 type I IFN signaling modulates T and B cell functions in lupus. We found previously that activation
84 of type I IFN can synergize with TCR signaling to promote the mechanistic target of rapamycin
85 (mTORC) 2 in T cells *in vitro*, which may contribute to Tfh cell-mediated immunopathology, and
86 T cell lymphopenia in lupus (16). Whether such IFN/ mTORC2 axis mediates lupus *in vivo* remains
87 unknown.
88
89 The mechanistic target of rapamycin (mTOR) is an evolutionally conserved serine/threonine
90 kinase complex regulating various cellular processes including growth, survival, and metabolism.
91 mTOR has two forms of complexes, mTORC1 and mTORC2, which play indispensable but
92 distinct roles in T cell biology. mTORC1 is critical for naïve T cell activation, proliferation, and
93 effector T cell differentiation (17), while mTORC2 mediates Tfh cell differentiation (18). In
94 regulatory T cells, mTORC1 maintains natural or thymic-derived Treg while overactivation of
95 mTORC2 suppresses Treg function and the ability of Tfh cell inhibition (19). Thus, mTORC2
96 activities regulate Tfh and Treg balance which can be critical in autoimmune diseases such as SLE.
97 We previously showed that the genetic deletion of mTORC2 in $CD4^+$ T cells in C57BL/6-Fas^{lpr}
98 (Lpr) mice, a lupus-prone mice, showed improved immunopathology associated with reduced Tfh
99 differentiation and glucose metabolism (16). Here, we provide evidence that mTORC2 deficiency
100 can ameliorate TLR7 agonist induced lupus development, which is associated with high type I IFN

signature and dependent on pDC (20). We also found that type I IFN receptor deficient Lpr mice have reduced mTORC2 activities linking to ameliorated lupus-like symptoms. Finally, we showed that pharmacological targeting mTORC2 can benefit lupus-like mice *in vivo* and reduce autoantibodies production in an *in vitro* co-culture system using T and B cells from SLE patients. Together, our results support that targeting mTORC2 in T cells could be a therapeutic option for SLE.

Material and Method

Mice

Cd4^{Cre}*Rictor*$^{fl/fl}$ mice have been described before (18). *Ifnar1*$^{-/-}$ (Strain #: 028288), C57BL/6-Fas^{lpr} (Lpr) (Strain #: 000482) and MRL/MpJ-Fas^{lpr}/J (MRL/*lpr*) (Strain #: 000485) mice were purchased from the Jackson Laboratory. *Ifnar1*$^{-/-}$ mice were crossed with C57BL/6-Fas^{lpr} mice to generate C57BL/6-Fas^{lpr}*Ifnar1*$^{-/-}$ mice. A total of 82 mice were used in this study, with a mix of male and female mice on *Cd4*^{Cre}*Rictor*$^{fl/fl}$ background, and female only mice on Fas^{lpr} background. MRL/*lpr* mice used for therapeutic testing were randomly allocated into different experimental groups. Mice were housed under specific pathogen-free conditions on a 12:12-h day: night cycle with access to normal chow (LabDiet, 5P76) and water. The room temperature was 22 ± 1 °C, with 31% humidity. All mice were bred and maintained in the Department of Comparative Medicine at Mayo Clinic Rochester. All animal procedures were approved by the Institutional Animal Use and Care Committee (IACUC).

Human sample collection/storage

Five SLE patients (53.6 ± 4.15 years) and five age-matched healthy donors' (55 ± 5.01 years) blood samples were collected for peripheral blood mononuclear cells (PBMC) isolation. PBMCs were isolated using Ficoll density gradient centrifugation and cryopreserved in liquid nitrogen until use. SLE patients fulfill the EULAR/ACR SLE 2019 criteria (21). Patients' demographics, disease manifestations and medications were detailed in Supplementary Table 1. The disease activity index was assessed using the Systemic Lupus Erythematosus Disease Activity Index 2000 (SLEDAI-2K) based on the manifestations presented one month before sample collection (22).

131

132 ASO Treatment

133 Ionis Pharmaceutical manufactured anti-mouse *Rictor*-ASO and anti-human *RICTOR*-ASO and
134 corresponding Ctrl-ASO. Each mouse received *Rictor*- or Ctrl-ASO subcutaneously at 50 mg/kg
135 once per week. Mice were treated for 6 consecutive weeks. Mouse proteinuria was measured
136 weekly by Urine Reagent Strips (Siemens).

137

138 Flow Cytometry

139 Single cell suspension of spleen and peripheral lymph nodes was prepared as previously described
140 (18). Cells were first stained with Fixable Dye Ghost 510 (Tonbo Bioscience) for viability, then
141 with desired surface marker antibodies on ice for 30 mins. Antibodies used are detailed in
142 supplementary methods. FACS data was acquired by the Attune NxT (ThermoFisher) cytometer.
143 Data analysis was performed in FlowJo software (Tree Star).

144

145 ELISA

146 ELISA was used to detect serum autoantibody levels. Briefly, 96-well plates (2596; Costar) were
147 coated with dsDNA (2 µg/ml in PBS), ssDNA (2 µg/ml in PBS), or chromatin (Sigma- Aldrich, 5
148 µg/ml) overnight at 4ºC. Plates were washed 4 times with PBS-T (0.05% Tween 20 in PBS) and
149 blocked with 5% blocking protein (Bio-Rad) at 37ºC for 1 h. Plates were then washed 4 times with
150 PBS-T before adding serially diluted serum. Serum coated plates were incubated at 37ºC for 1.5h.
151 Plates were next washed 8 times before horseradish peroxidase (HRP)-conjugated detection Abs
152 for IgG (Bethyl Laboratories). Coated plates were incubated at 37ºC for another 1.5h, washed 8
153 times, and added tetramethylbenzidine (TMB) substrate. The reaction is stopped by 2N H_2SO_4 and

read at 450nm by a plate reader. Mouse serum and detection antibodies were diluted in dilution buffer (1% BSA in PBS-T).

Immunoblotting

Mouse $CD4^+$ T cells were enriched from lymph node single-cell solution using EasySep™ Mouse $CD4^+$ T Cell Isolation Kit (STEMCELL, Cat # 19852). Human $CD4^+$ T cells were enriched from PBMCs using EasySep™ Human $CD4^+$ T Cell Isolation Kit (STEMCELL, Cat # 17952). The same numbers of cells from each sample were used for the experiment. Cells were lysed in RIPA lysis buffer (Sigma). Lysed protein concentrate was used for electrophoresis and membrane transfer. The transferred membrane was first blocked with 5% milk in TBST (0.1% Tween 20) for 1h at room temperature, washed, and incubated with primary antibodies overnight. The following primary antibodies have been used: anti-phospho-AKT (Ser473) (D9E), AKT (pan) (40D4), anti-p-S6 (Ser235/Ser236, D57.2.2E), anti-RICTOR (53A2) and anti-b-actin (13E5). The next day, the membrane was washed and incubated with corresponding secondary antibodies for subsequent enhanced chemiluminescence (ECL; Thermo Fisher) exposure. Images were captured on an Azure Imaging system. Blot intensity was quantified using ImageJ software.

Metabolic assay

Mouse $CD4^+$ T cells were enriched using EasySep™ Mouse $CD4^+$ T Cell Isolation Kit (STEMCELL, Cat # 19852). Isolated cells were activated with plate-coated anti-CD3 (2 µg/ml, Bio X Cell) and anti-CD28 (2 µg/ml, Bio X Cell) for 48h, and rested overnight without stimulation. Live cells were purified with lymphocyte isolation buffer (MP Biomedicals) and then restimulated with plate-coated anti-CD3 (2 µg/ml) and anti-ICOS (5 µg/ml, Biolegend, Cat# 313502) for 24 h.

Metabolic activities of ICOS-stimulated cells were then measured by the SCENITH method (23); a detailed description is provided in supplementary methods.

T-B cell coculture assay

T-B coculture assay was performed as previously described (24). Detailed description of the assay is provided in the supplementary methods. Coculture supernatant was collected for immunoglobulin isotypes and autoantigen detection. Autoantigen microarray was performed by Genecopoeia Inc.

Immunoglobulin isotypes detection

Mouse (IgG1, IgG2a, IgG2b, IgG3, IgA, IgM) and human (IgG1, IgG2, IgG3, IgG4, IgA, IgM) immunoglobulin isotypes were measured by LEGENDplex mouse immunoglobulin isotyping panel (Biolegend; cat# 740493) and human Immunoglobulin Isotyping Panel (6-plex) (Biolegend; cat# 740639) respectively following the manufacturer's instructions.

Inflammatory cytokines detection

Mouse serum cytokine level was measured by LEGENDplex Mouse Inflammation Panel (Biolegend, cat# 740446) according to the manufacturer's instructions.

Statistical analysis

All data are presented as mean ± SEM. One-way analysis of variance (ANOVA) with post-hoc Tukey test was used for multiple groups comparison. Unpaired and paired student t-tests was used for two groups comparison. The Kaplan-Meier survival analysis was used to compare the survival

probability differences among groups. Detailed statistical tests are described in individual figure legends. Statistical analysis and graph generation were performed in GraphPad Prism version 9.0.

Results

Mice with T cell specific *Rictor* deletion develop less systemic inflammation upon TLR7 agonist challenge.

We previously demonstrated that loss of mTORC2 in T cells substantially alleviates autoimmunity in C57BL/6-Fas^{lpr} (Lpr) mice (16). However, Lpr mice do not develop overt kidney pathology. Toll-like receptor (TLR) 7 signaling is known to contribute to lupus initiation and exacerbation in humans (25) and mice (26). Topical application of a TLR7 agonist, imiquimod (IMQ), induces lupus-like symptoms with tissue pathology in C57BL/6 (WT) mice (20). To study whether the loss of mTORC2 signaling in T cells may impact TLR7 induced SLE development in mice, we topically administered IMQ on *Cd4*^{Cre}*Rictor*$^{fl/fl}$ mice. Following 6 weeks of IMQ application, *Cd4*^{Cre}*Rictor*$^{fl/fl}$ mice had a lower spleen weight than their WT counterparts (Figure 1A). Flow cytometry analysis of splenocytes showed that *Cd4*^{Cre}*Rictor*$^{fl/fl}$ mice had a significantly lower percentage of T-bet^{+}B220^{+} and CD11c^{+}B220^{+} age-associated B cells (ABCs) (Figure 1B, supplementary Figure 1A), germinal center (GC) B cells (Figure 1C) and plasma cells (Figure 1D), indicating overall attenuated B cell activation. Correspondingly, a higher percentage of naïve B cells was seen in *Cd4*^{Cre}*Rictor*$^{fl/fl}$ mice (Supplementary Figure 1B). While no change of marginal zone B cells was observed (Supplementary Figure 1C), a lower percentage of Bcl6 expressing B cells (Supplementary Figure 1D) was seen in *Cd4*^{Cre}*Rictor*$^{fl/fl}$ mice. Additionally, there was a lower percentage of Tfh cells (Figure 1E) and CD44^{hi}CD62^{low} effector CD4^{+} T cells (Figure 1F) in *Cd4*^{Cre}*Rictor*$^{fl/fl}$ mice. Little change of Foxp3^{+} Treg cells (Supplementary Figure 1E) was seen between two groups of mice, while *Cd4*^{Cre}*Rictor*$^{fl/fl}$ mice had fewer T-bet expressing CD4^{+} T cells (Supplementary Figure 1F). We also observed reduced plasmacytoid dendritic cells (pDCs) (Supplementary Figure 1G) in *Cd4*^{Cre}*Rictor*$^{fl/fl}$ mice, a population has been reported critically

linked to lupus development (27). Other myeloid cell populations including cDC, monocytes and neutrophils remained unchanged (Supplementary Figure 1 G-J). These data were consistent with previous observations that mTORC2 critically contributes to humoral immunity in Lpr mice (16). They further indicate that mTORC2 in T cells could be required for the formation of ABC, a B cell lineage critical for TLR7 mutation mediated lupus pathogenesis (28). To assess systemic inflammation, we quantified inflammatory cytokines in the serum of IMQ treated mice. *Cd4*^{Cre}*Rictor*$^{fl/fl}$ mice had lower levels of cytokines such as IL1α, IFNβ, IFNγ, IL23, and IL27 (Figure 1G), commonly associated with lupus pathogenesis in both murine models and humans (29). ELISA measurements also showed that *Cd4*^{Cre}*Rictor*$^{fl/fl}$ mice had lower levels of anti-dsDNA and anti-histone antibodies than their WT counterparts (Figure 1H). Finally, kidney histology showed that WT mice developed moderate glomerulosclerosis with mesangial thickening, which were significantly improved in *Cd4*^{Cre}*Rictor*$^{fl/fl}$ mice, indicating a less extent of kidney damage (Figure 1I). Taken together, these results indicate that mTORC2 deficiency in T cells effectively impedes the immunopathologic transition in IMQ-induced lupus model.

IFNAR1 deletion partially inhibits mTORC2 activities in T cells and restores TCR/ICOS-mediated glucose metabolism in Lpr CD4$^+$ T cells.

We previously showed that type I IFNs synergize with TCR signaling to active mTORC2 *in vitro* (16). Thus, we hypothesized that elevated type I IFN signaling in SLE contributes to mTORC2 activation *in vivo*, which promotes disease development. To test this hypothesis, we generated IFNAR1 deficient Lpr (Lpr-*Ifnar1*$^{-/-}$) mice and investigated mTORC2 activities in these mice. To directly evaluate the mTORC2 activation in CD4$^+$ T cells, we performed immunoblot on purified CD4$^+$ T cells derived from different groups of mice. Elevated phosphorylated AKT (p-AKT) S473

expression, the direct target of mTORC2, was seen in Lpr T cells, which was reduced in T cells from Lpr-*Ifnar1*$^{-/-}$ mice (Figure 2A), indicating reduced mTORC2 activation in CD4^{+} T cells of Lpr-*Ifnar1*$^{-/-}$ mice. mTORC2 is known to modulate CD69 surface expression on CD4^{+} T cells (18). We previously showed that mTORC2 is required for the increased CD69 expression on Lpr T cells, which partially contributes to T cell lymphopenia phenotype in Lpr mice (16). As expected, IFNAR1 deficiency led to reduced CD69 expression in Lpr CD4^{+} T cells in blood (Figure 2B) and peripheral lymph nodes (pLN) (Supplementary Figure 2A), as well as increased CD4^{+} T cell frequency in both blood (Figure 2C) and pLN (Supplementary Figure 2B) in Lpr mice. These results are consistent with our hypothesis that type I IFN contributes to mTORC2 activation in CD4 T cells, and with the clinical observation that type I IFN signature is strongly associated with CD4 T cell lymphopenia in SLE patients (30) . mTORC2 is also critical for TCR/ICOS-mediated glucose metabolism (18). Following TCR/ICOS stimulation *in vitro*, Lpr CD4^{+} T cells have significantly increased glycolytic capacities than WT cells, and such increase was significantly reduced in the absence of IFNAR1 (Figure 2D). Interestingly, we also observed partially restored proliferation in Lpr-*Ifnar1*$^{-/-}$ CD4^{+} T cells (Figure 2E). Because mTORC2 deletion does not restore CD4^{+} T cell proliferation in Lpr mice, type I IFN likely modulates CD4^{+} T cell proliferation independent of mTORC2 signaling. Despite the partial rescue on glucose metabolism and proliferation, IFNAR1 deletion has little rescue effect on the apoptosis of CD4^{+} T cells in Lpr mice (Figure 2F). In summary, IFNAR1 deficiency led to reduced mTORC2 activity and mTORC2-mediated T cell lymphopenia and glucose metabolism in Lpr mice.

IFNAR1 deletion rescues immunopathology in C57BL/6-Fas^{lpr} mice.

Elevated interferon signature has been identified in both SLE patients (7) and lupus-prone mice (31). However, type I IFNAR deletion or inhibition yields controversial outcomes in Lpr and MRL/*lpr* mice (12,13). We revisited this question and examined the mTORC2-associated immunophenotype changes in Lpr-*Ifnar1*$^{-/-}$ mice. Compared to Lpr mice, Lpr-*Ifnar1*$^{-/-}$ mice had smaller sizes of peripheral lymph nodes and yielded a lower number of lymphocytes (Figure 3A). Lpr-*Ifnar1*$^{-/-}$ mice had lower levels of anti-dsDNA (Figure 3B) and lower concentrations of immunoglobulin isotypes including IgG1, IgG2a, and IgA than those from Lpr mice (Figure 3C). Furthermore, IFNAR1 deficiency reduced serum concentrations of multiple inflammatory cytokines, including TNFα, MCP1, IFNβ, IL17A, and IL23 (Figure 3D). The abnormal immune phenotypes presented in Lpr mice such as accumulated aberrant B220^{+}TCRβ^{+} cells (Figure 3E) and CD4^{-}CD8^{-}DN cells (Figure 3F), modestly but significantly reduced in Lpr-*Ifnar1*$^{-/-}$ mice. Reflecting reduced autoantibodies and immunoglobulin levels, Lpr-*Ifnar1*$^{-/-}$ mice have reduced CD138^{+}B220^{int} population (Supplementary Figure 2C) and reduced Bcl6 expression in B220^{+} cells than Lpr mice, suggesting reduced antibody-producing plasma lineage cells and reduced GC B cell activities (Supplementary Figure 2D). mTORC2 is known to promote Tfh cell differentiation (18). We observed a reduced CXCR5^{+}PD-1^{hi} cell population in Lpr-*Ifnar1*$^{-/-}$ mice (Figure 3G). Lpr-*Ifnar1*$^{-/-}$ mice did not show significantly reduced ICOS expression on CD4^{+} T cells (Supplementary Figure 2E) but had a significantly lower percentage of CXCR5^{+}Bcl6^{+} and CXCR5^{+}Bcl6^{-} populations than Lpr mice (Supplementary Figure 2G), reminiscent of the phenotypes of Lpr mice with T cell specific deletion of *Rictor* (16). mTORC2 activation is also known to suppress Treg function (19). However, Treg frequency was not significantly altered in Lpr-*Ifnar1*$^{-/-}$ mice compared to Lpr mice (Supplementary Figure 2F), suggesting that type I IFN signaling might not substantially affect Treg homeostasis in Lpr mice. Together, our results

293 demonstrated that IFNAR1 deficiency partially rescues autoimmune phenotypes in Lpr mice,
294 associated with reduced systemic inflammation, Tfh differentiation and B cell activation,
295 associated with reduced mTORC2 activity. Our data reaffirms the disease promoting function of
296 type I IFN in Lpr mice and provides evidence of association between type I IFN and mTORC2
297 signaling in SLE.
298
299 **_Rictor_-ASO treatment benefits lupus-like symptoms in MRL/_lpr_ mice.**
300 After demonstrating that genetic targeting mTORC2 in T cells ameliorates SLE in mouse models
301 and the close link between mTORC2 and type IFN signaling in SLE development, we sought to
302 target mTORC2 pharmacologically. We designed antisense oligonucleotides (ASOs) that
303 specifically targets mouse *Rictor*. Immunoblot analysis showed that anti-mouse *Rictor*-ASO could
304 effectively delete RICTOR and abrogate AKT phosphorylation at S473 site in mouse $CD4^+$ T cells
305 without affecting mTORC1 signaling (Figure 4A). We next tested if *Rictor*-ASO exhibited
306 beneficial effects in MRL/*lpr* mice (Figure 4B), a mouse strain with spontaneous lupus-like
307 symptoms commonly used for SLE therapeutic testing. We observed that *Rictor*-ASO could
308 significantly improve the survival probability of MRL/*lpr* mice (Figure 4C) and reduce proteinuria
309 levels in those mice (Figure 4D) than Ctrl-ASO. At 19 weeks, *Rictor*-ASO treated mice had lower
310 creatinine concentration in both urine (Figure 4E) and serum (Figure 4F), as well as reduced serum
311 urea nitrogen concentration (Figure 4G) than in Ctrl-ASO treated mice, suggesting improved renal
312 function. *Rictor*-ASO treated mice also had smaller pLN (Supplementary Figure 3A). Flow
313 analysis showed that *Rictor*-ASO treatment increased the percentage of $CD4^+$ T cells in pLN of
314 MRL/*lpr* mice (Supplementary Figure 3B). Decreased CD69 expressing $CD4^+$ T cells were also
315 observed in *Rictor*-ASO treated mice (Supplementary Figure 3C), consistent with our data from

316 genetic models. We also detected lower autoantibody (Figure 4H) and immunoglobulin isotype
317 levels in serum (Figure 4I) in *Rictor*-ASO treated mice, indicating reduced humoral immune
318 activation. Reduced levels of inflammatory cytokines in *Rictor*-ASO treated mice suggested
319 reduced systemic inflammation (Figure 4J). Finally, kidney histology revealed that *Rictor*-ASO
320 treated mice have a lower number of foci and a lower level of cortex inflammation than Ctrl-ASO
321 treated mice at 19 weeks (Figure 4K), indicating less extent of nephritis. Taken together, these data
322 indicate that *Rictor*-ASO treatment can enhance survival and ameliorate lupus-like diseases in
323 MRL/*lpr* mice.
324
325 ***RICTOR*-ASO treated SLE patient derived Tfh-like cells reduce antibody production in T:B**
326 **coculture assay.**
327 Aberrant mTORC2 activation and increased circulating Tfh-like cells have been shown to strongly
328 correlate with disease activity in SLE patients (32,33). We finally asked if targeting mTORC2
329 using human *RICTOR*-ASO in human SLE Tfh cells can reduce B cell activities *in vitro*. We
330 showed that *RICTOR*-ASO could effectively reduce RICTOR expression and mTORC2 activity in
331 human $CD4^+$ T cells (Figure 5A). To test whether inhibition of mTORC2 in Tfh cells can reduce
332 Tfh mediated antibody production *in vitro,* we sorted Tfh-like cells ($CD4^+CXCR5^+PD\text{-}1^+CXCR3^-$)
333 from SLE patients' (53.6 ± 4.15 years) PBMCs. After treating sorted Tfh cells with *RICTOR*-/Ctrl-
334 ASO for 5 days, memory B cells ($CD19^+IgD^-CD27^+$ $CD38^-$) sorted from the same donor-matched
335 SLE PBMCs were cocultured with ASO-treated Tfh cells for 7 days (Figure 5B). SLE patients'
336 demographics and disease characteristics were shown in Supplementary Table 1. At day 7, we
337 observed substantially lower immunoglobulin isotypes (i.e. IgG1, IgG3, IgG4, IgM) in the
338 supernatant of *RICTOR*-ASO treated SLE T-B cocultures than those of the Ctrl-ASO counterparts

(Figure 5C). Reduced IgG1 and IgG4, but not other, immunoglobulin level was also seen in *RICTOR*-ASO treated T-B coculture derived from age-matched healthy donor (HC, 55 ± 5.01 years) PBMCs (Supplementary Figure 4). Autoantigen array showed significantly reduced autoantibodies signal against various autoantigens, such as Lo/SSO and Ra/SSA, in *RICTOR*-ASO treated SLE T-B coculture compared to paired Ctrl-ASO counterparts (Figure 5D, E). These data suggest that targeting mTORC2 in SLE patient Tfh cells could effectively reduce immunoglobulin isotypes and autoantibodies production, highlighting a promising therapeutic potential in clinics.

Discussion

In this study, we tackled the contribution of mTORC2 in T cells for lupus disease development, investigated the relationship between mTORC2 and type I IFN in SLE pathogenesis, and explored the therapeutic potential of mTORC2 targeting ASOs in mice and humans. We showed that genetic deletion of RICTOR in mice can effectively ameliorate IMQ-induced lupus-like diseases. We also found that the loss of IFNAR1 in Lpr mice correlates with reduced mTORC2 activities. Finally, we developed novel anti-mouse *Rictor*- and anti-human *RICTOR*-ASO that efficiently and specifically suppress mTORC2. Anti-mouse *Rictor*-ASO can delay disease onset and benefit lupus nephritis in MRL/*lpr* mice. Inhibiting RICTOR expression in human SLE patient derived Tfh-like cells by anti-human *RICTOR*-ASO can reduce immunoglobulin isotypes and autoantibodies production in an *in vitro* T-B coculture system. These results showed that mTORC2 plays a pivotal role in SLE disease development and interconnected with known molecular pathways in SLE pathogenesis. Therefore, targeting the mTORC2 pathway using ASOs could be an effective therapeutic for future SLE management.

Both type I and type II IFN signaling dysregulation have been reported in human SLE (34). However, how IFN signaling regulates $CD4^+$ T cell differentiation and trafficking in SLE is not fully understood. Gain-of-function genetic variants in both type I and II IFN pathways have been identified as risk factors for SLE (35,36). Type I IFN signaling has been recognized as a key player in SLE pathogenesis with elevated IFNα and IFNg gene signatures as hallmarks of human SLE (37), and anti-IFN-α/β receptor antibodies can reduce lupus-like symptoms in mice (14) and humans (38). One of the intriguing findings from a large-scale single cell RNAseq analysis of 162 SLE patients is that type I IFN signature is highly correlated with $CD4^+$ T cell lymphopenia,

correlates with the known function of type I IFN-CD69 axis on T cell egress (30,39). Consistent with this observation, treatment with anifrolumab, an IFNAR1 antagonist, is associated with correction of T cell lymphopenia symptom in SLE patients (40). Our investigation builds on earlier study and provides potential immunological mechanisms through which type I IFN may contribute to SLE. Our data corroborates with the clinical observation that type I IFN activation partially contributes to $CD4^+$ T cell lymphopenia, overactivation of Tfh, GC and extrafollicular responses. Importantly, type I IFN activation is also associated with mTORC2 activation and increased T cell glucose metabolism in Lpr mouse model. Indeed, the immunological phenotypes of Lpr-*Ifnar1*$^{-/-}$ mice closely resemble those of Lpr-*Rictor* T-KO mice, including the partial rescue of CD69 expression, $CD4^+$ T cell lymphopenia, Tfh/GC differentiation (without affecting ICOS expression on T cells) and T cell glucose metabolism. Overall, the magnitude of rescue is stronger in Lpr-*Rictor* T-KO mice than in Lpr-*Ifnar1*$^{-/-}$ mice, suggesting that factors other than IFNAR1 signal through mTORC2 in Lpr mice. These results highlighted the close relation between mTORC2 signaling and classic SLE pathogenic signaling, further indicating its indispensable role in SLE development.

While mTORC2 activities are known to elevate in human SLE (41), the lack of selective mTORC2 inhibitors has long hindered functional studies and therapeutic development. RNA-based silencing technique showed the feasibility of specific silencing of RICTOR and corresponding therapeutic effects in a breast cancer model (42), pointing the direction of mTORC2-based therapies. ASOs have emerged as the new generation of therapies for a wide range of rare diseases such as neurological, inherited metabolic, and infectious diseases (43). ASO targeting mTORC2 was first successfully used to ameliorate a neurological disorder induced by brain-specific loss of PTEN

(44). Our results showed that mTORC2 targeting ASOs can effectively and specifically suppress mTORC2 in both human and mouse $CD4^+$ T cells. Administration of *RICTOR*-ASO in MRL/*lpr* mice can improve mice survival, kidney function, and immunopathology, suggesting its promising therapeutic potential. Further, we showed that reducing RICTOR expression by anti-human *RICTOR*-ASO in human SLE Tfh cells can reduce immunoglobulin and autoantibodies production when cocultured with donor-matched memory B cells. These results further support the idea of using *RICTOR*-ASOs for human SLE management. Given the heterogeneity of human SLE, it is crucial to map the mTORC2 signature in larger-scale patient populations in future studies to enable individualized mTORC2-based therapy. Given the relatively narrow immunological impact of mTORC2 inhibition compared to mTORC1 inhibition (19), it is plausible that targeting mTORC2 specifically could have fewer immune suppressive side effects than mTORC1 inhibition. Future comparative studies are warranted to address this question.

In summary, our study provides mechanistic insight that associates mTORC2 with type I IFN signaling in lupus immunopathology. We further provide proof-of-principle evidence that ASO mediated mTORC2 inhibition could ameliorate lupus symptoms using lupus mouse model and *in vitro* T-B cell co-culture derived from SLE patients. Future pre-clinical and clinical studies will be needed to identify mTORC2 signatures in heterogeneous SLE patients and test the safety and efficacy of ASO treatment for human SLE.

Acknowledgment

We acknowledge Mayo Clinic Arizona Histology Core Laboratory for the process and histological staining of mouse kidney specimens. We acknowledge Genecopoeia Inc. for autoantigen array analysis. The study is supported by NIH R01AR077518 and R01AI162678 (to H.Z.), lupus Research Alliance (696599, to H.Z.) and Mayo Foundation for Medical Education and Research.

Author contributions

All the authors were involved in drafting or revising the article critically for important intellectual content, and all authors approved the final version to be published. Dr. Zeng has full access to all the data in the study and takes responsibility for the integrity of the data and the accuracy of the data analysis. M.A. and H.Z. conceived the study, designed the experiments and wrote the manuscript. M.A., X.Z. and Y.L. prepared the research material and carried out the experiments. M.C. and P.J. designed and provided the control, anti-*Rictor* and anti-*RICTOR* ASOs. M.A.B. and A.A.D.G analyzed patient clinical data. N.G. and M.A. performed the pathological review.

Conflict of interest

MC and PJ are paid employees of Ionis Pharmaceuticals.

Reference

1. Tian J, Zhang D, Yao X, et al. Global epidemiology of systemic lupus erythematosus: a comprehensive systematic analysis and modelling study. *Ann Rheum Dis* 2023;82:351–356.

2. Siegel CH, Sammaritano LR. Systemic Lupus Erythematosus. *JAMA* 2024;331:1480–1491.

3. Sigdel KR, Thapa A, Dahal A, et al. Azathioprine-induced pancytopenia: A case report. *Rheumatol Autoimmun* 2022;2:179–184.

4. Kirou KA, Dall`Era M, Aranow C, et al. Belimumab or anifrolumab for systemic lupus erythematosus? A risk-benefit assessment. *Front Immunol* 2022;13:980079.

5. Sutanto H, Yuliasih Y. Disentangling the Pathogenesis of Systemic Lupus Erythematosus: Close Ties between Immunological, Genetic and Environmental Factors. *Medicina* 2023;59:1033.

6. Crow MK. Pathogenesis of systemic lupus erythematosus: risks, mechanisms and therapeutic targets. *Ann Rheum Dis* 2023;82:999–1014.

7. Murayama G, Furusawa N, Chiba A, et al. Enhanced IFN-α production is associated with increased TLR7 retention in the lysosomes of palasmacytoid dendritic cells in systemic lupus erythematosus. *Arthritis Res Ther* 2017;19:234.

8. Kiefer K, Oropallo MA, Cancro MP, et al. Role of type I interferons in the activation of autoreactive B cells. *Immunol Cell Biol* 2012;90:498–504.

449 9. Mathian A, Weinberg A, Gallegos M, et al. IFN-α Induces Early Lethal Lupus in
450 Preautoimmune (New Zealand Black × New Zealand White)F1 but Not in BALB/c Mice. *J*
451 *Immunol* 2005;174:2499–2506.

452 10. Nacionales DC, Kelly-Scumpia KM, Lee PY, et al. Deficiency of the type I interferon
453 receptor protects mice from experimental lupus. *Arthritis Rheum* 2007;56:3770–3783.

454 11. Santiago-Raber M-L, Baccala R, Haraldsson KM, et al. Type-I Interferon Receptor
455 Deficiency Reduces Lupus-like Disease in NZB Mice. *J Exp Med* 2003;197:777–788.

456 12. Braun D, Geraldes P, Demengeot J. Type I Interferon controls the onset and severity of
457 autoimmune manifestations in lpr mice. *J Autoimmun* 2003;20:15–25.

458 13. Hron JD, Peng SL. Type I IFN Protects Against Murine Lupus. *J Immunol* 2004;173:2134–
459 2142.

460 14. Baccala R, Gonzalez-Quintial R, Schreiber RD, et al. Anti–IFN-α/β Receptor Antibody
461 Treatment Ameliorates Disease in Lupus-Predisposed Mice. *J Immunol* 2012;189:5976–5984.

462 15. Baker T, Sharifian H, Newcombe PJ, et al. Type I interferon blockade with anifrolumab in
463 patients with systemic lupus erythematosus modulates key immunopathological pathways in a
464 gene expression and proteomic analysis of two phase 3 trials. *Ann Rheum Dis* 2024:ard-2023-
465 225445.

466 16. Zhou X, Qi H, Li M, et al. mTORC2 contributes to systemic autoimmunity. *Immunology*
467 2023;168:554–568.

468 17. Chi H. Regulation and function of mTOR signalling in T cell fate decisions. *Nat Rev*
469 *Immunol* 2012;12:325–338.

470 18. Zeng H, Cohen S, Guy C, et al. mTORC1 and mTORC2 Kinase Signaling and Glucose
471 Metabolism Drive Follicular Helper T Cell Differentiation. *Immunity* 2016;45:540–554.

472 19. Zeng H, Chi H. mTOR signaling in the differentiation and function of regulatory and effector
473 T cells. *Curr Opin Immunol* 2017;46:103–111.

474 20. Yokogawa M, Takaishi M, Nakajima K, et al. Epicutaneous Application of Toll-like
475 Receptor 7 Agonists Leads to Systemic Autoimmunity in Wild-Type Mice: A New Model of
476 Systemic Lupus Erythematosus. *Arthritis Rheumatol* 2014;66:694–706.

477 21. Aringer M, Costenbader K, Daikh D, Brinks R, et al. 2019 European League Against
478 Rheumatism/American College of Rheumatology Classification Criteria for Systemic Lupus
479 Erythematosus. *Arthritis Rheumatol* 2019;71:1400–1412.

480 22. Gladman DD, Ibañez D, Urowitz MB. Systemic lupus erythematosus disease activity index
481 2000. *J Rheumatol* 2002;29:288–91.

482 23. Argüello RJ, Combes AJ, Char R, et al. SCENITH: A Flow Cytometry-Based Method to
483 Functionally Profile Energy Metabolism with Single-Cell Resolution. *Cell Metab* 2020;32:1063-
484 1075.e7.

485 24. Locci M, Havenar-Daughton C, Landais E, et al. Human Circulating PD-
486 1+CXCR3−CXCR5+ Memory Tfh Cells Are Highly Functional and Correlate with Broadly
487 Neutralizing HIV Antibody Responses. *Immunity* 2013;39:758–769.

488 25. Brown GJ, Cañete PF, Wang H, et al. TLR7 gain-of-function genetic variation causes human
489 lupus. *Nature* 2022;605:349–356.

490 26. Christensen SR, Shupe J, Nickerson K, et al. Toll-like Receptor 7 and TLR9 Dictate
491 Autoantibody Specificity and Have Opposing Inflammatory and Regulatory Roles in a Murine
492 Model of Lupus. *Immunity* 2006;25:417–428.

493 27. Chan VS-F, Nie Y-J, Shen N, et al. Distinct roles of myeloid and plasmacytoid dendritic cells
494 in systemic lupus erythematosus. *Autoimmun Rev* 2012;11:890–897.

495 28. Dai D, Gu S, Han X, et al. The transcription factor ZEB2 drives the formation of age-
496 associated B cells. *Science* 2024;383:413–421.

497 29. Su D-L, Lu Z-M, Shen M-N et al. Roles of Pro- and Anti-Inflammatory Cytokines in the
498 Pathogenesis of SLE. *J Biomed Biotechnol* 2012;2012:347141.

499 30. Perez RK, Gordon MG, Subramaniam M, et al. Single-cell RNA-seq reveals cell type–
500 specific molecular and genetic associations to lupus. *Science* 2022;376:eabf1970.

501 31. Zhuang H, Szeto C, Han S, et al. Animal Models of Interferon Signature Positive Lupus.
502 *Front Immunol* 2015;6:291.

503 32. Choi J, Ho JH, Pasoto SG, et al. Circulating Follicular Helper–Like T Cells in Systemic
504 Lupus Erythematosus: Association With Disease Activity. *Arthritis Rheumatol* 2015;67:988–
505 999.

506 33. Suárez-Fueyo A, Barber DF, Martínez-Ara J, et al. Enhanced Phosphoinositide 3-Kinase δ
507 Activity Is a Frequent Event in Systemic Lupus Erythematosus That Confers Resistance to
508 Activation-Induced T Cell Death. *J Immunol* 2011;187:2376–2385.

509 34. Sirobhushanam S, Lazar S, Kahlenberg JM. Interferons in Systemic Lupus Erythematosus.
510 *Rheum Dis Clin North Am* 2021;47:297–315.

511 35. Siddiqi KZ, Zinglersen AH, Iversen KK, et al. A cluster of type II interferon-regulated genes
512 associates with disease activity in patients with systemic lupus erythematosus. *J Autoimmun*
513 2022;132:102869.

514 36. Ghodke-Puranik Y, Niewold TB. Genetics of the type I interferon pathway in systemic lupus
515 erythematosus. *Int J Clin Rheumatol* 2013;8:657–669.

516 37. Bradford HF, Haljasmägi L, Menon M, et al. Inactive disease in patients with lupus is linked
517 to autoantibodies to type I interferons that normalize blood IFNα and B cell subsets. *Cell Rep*
518 *Med* 2023;4:100894.

519 38. Riggs JM, Hanna RN, Rajan B, et al. Characterisation of anifrolumab, a fully human anti-
520 interferon receptor antagonist antibody for the treatment of systemic lupus erythematosus. *Lupus*
521 *Sci Med* 2018;5:e000261.

522 39. Cyster JG, Schwab SR. Sphingosine-1-Phosphate and Lymphocyte Egress from Lymphoid
523 Organs. *Immunology* 2012;30:69–94.

524 40. Casey KA, Guo X, Smith MA, et al. Type I interferon receptor blockade with anifrolumab
525 corrects innate and adaptive immune perturbations of SLE. *Lupus Sci Med* 2018;5:e000286.

526 41. Kato H, Perl A. Mechanistic Target of Rapamycin Complex 1 Expands Th17 and IL-4+
527 CD4−CD8− Double-Negative T Cells and Contracts Regulatory T Cells in Systemic Lupus
528 Erythematosus. *J Immunol* 2014;192:4134–4144.

529 42. Werfel TA, Wang S, Jackson MA, et al. Selective mTORC2 inhibitor therapeutically blocks
530 breast cancer cell growth and survival. *Cancer Res* 2018;78:canres.2388.2017.

531 43. Lauffer MC, Roon-Mom W van, Aartsma-Rus A, Collaborative N= 1. Possibilities and
532 limitations of antisense oligonucleotide therapies for the treatment of monogenic disorders.
533 *Commun Med* 2024;4:6.

534 44. Chen C-J, Sgritta M, Mays J, et al. Therapeutic inhibition of mTORC2 rescues the behavioral
535 and neurophysiological abnormalities associated with Pten-deficiency. *Nat Med* 2019;25:1684–
536 1690.

537

538 **Figure Legend**

539

540 **Figure 1: Mice with RICTOR deletion in T cells develop less severe lupus-like diseases**
541 **following imiquimod (IMQ) treatment.** WT and *Cd4*^{cre}*Rictor*$^{fl/fl}$ mice were treated with IMQ
542 epicutaneously 3 times a week for 6 weeks. (A) Spleen size (left) and weight (right) of IMQ-treated
543 mice. (B) Expression of T-bet and B220 in splenocytes. Right, summary of T-bet^{+}B220^{+} age-
544 associated B cell frequencies. (C) Expression of CD95 and GL7 on splenocytes. Right, summary
545 of CD95^{+}GL7^{+} germinal center B cell frequencies. (D) Expression of TACI and CD138 on
546 splenocytes. Right, summary of TACI^{+}CD138^{+} plasma cell frequencies. (E) Expression of CXCR5
547 and PD-1 on splenocytes. Right, summary of CXCR5^{+}PD-1^{hi} Tfh cell frequencies. (F) Expression
548 of CD62L and CD44 on CD4+ T cells from splenocytes. Right, summary of CD44^{+}CD62L^{-}
549 effector T cell frequencies. (G) The inflammatory cytokine levels in IMQ treated mouse serum.
550 (H) Antibody tiers of Anti-dsDNA and anti-histone antibodies in IMQ treated mouse serum
551 measured by ELISA. The serum was diluted at 1:100. (I) Representative H&E staining images of
552 kidneys. Right, summary of histology scores. Scale bar: 50 μm. *$p < 0.05$, **$p < 0.01$, ***$p<0.001$.
553 p-Values were calculated with unpaired t-tests. Error bars represent SEM.

554

555 **Figure 2: IFNAR1 deletion inhibits mTORC2 activity and rescues TCR/ICOS mediated**
556 **glucose metabolism in CD4^{+} T cells of Lpr mice.** (A) Immunoblot image (left) of p-AKT473 in
557 CD4^{+} T cells derived from the lymph nodes of 6-month-old B6, Lpr and Lpr.*Ifnar1*$^{-/-}$ *mice*. Right,
558 relative pAKT473 expression level normalized to AKT expression in each mouse. (B) Expression
559 of CD69 and CD4 on cells derived from peripheral blood. Right, summary of CD4^{+}CD69^{+} cell
560 frequencies. (C) Expression of B220 and CD4 in peripheral blood. Right, summary of B220^{+}CD4^{+}

cell frequencies. (D) Puromycin incorporation assay in $CD4^+$ T cells after sequential anti-CD3/anti-CD28, and anti-CD3/anti-ICOS stimulation. Left: glycolytic capacity of $CD4^+$ T cells after sequential stimulation; right: relative cell number change after sequential stimulation. Data were normalized to B6 in each experiment. (E) Representative flow plots of Cell trace violet (CTV) dilution in $CD4^+$ T cells after 3 days of anti-CD3/anti-CD28 stimulation. Left: proliferation index; right: absolute cell number after stimulation. (F) Flow staining of Annexin V and 7AAD on $CD4^+$ T cells after overnight stimulation of anti-CD3/anti-CD28. Left: frequency of early apoptotic cells; right: frequency of necrotic cells. 2-DG, 2-deoxyglucose; Oligo, Oligomycin. ns, not significant; *p < 0.05, **p < 0.01, ***p < 0.001, ****p < 0.0001. p-Values were calculated with one-way ANOVA with the post-hoc Tukey test. Error bars represent SEM.

Figure 3: IFNAR1 deletion reduces systemic inflammation in Lpr mice. (A) Representative image of peripheral lymph nodes (left) and cellularity (right) from 6 months B6, Lpr, and Lpr.*Ifna1r*$^{-/-}$ mice. (B) Tiers of anti-ssDNA antibody level in mice serum measured by ELISA. Serum immunoglobulin (Ig) isotype concentration (C) and inflammatory cytokine concentration (D) in 6-month-old mice. (E) Expression of TCRb and B220 in pLN derived lymphocytes. Left, frequency of $TCRb^+B220^+$ population; right absolute cell number of $TCRb^+B220^+$ cells in pLN. (F) Expression of CD4 and CD8 in pLN derived lymphocytes. Left, frequency of $CD4^-CD8^-$ population; right absolute cell number of $CD4^-CD8^-$ cells in pLN. (G) Expression of CXCR5 and PD-1 in pLN derived lymphocytes. Left, frequency of $CXCR5^+PD\text{-}1^{hi}$ Tfh cells; right, absolute cell number of $CXCR5^+PD\text{-}1^{hi}$ Tfh cells in pLN. ns, not significant; *p < 0.05, **p < 0.01, ***p < 0.001, ****p < 0.0001. p-Values were calculated with one-way ANOVA with post hoc Tukey test. Error bars represent SEM.

Figure 4: Anti-mouse *Rictor*-ASO treatment benefits lupus-like symptoms in MRL/*lpr* mice. (A) Immunoblot image showing the deletion of RICTOR by *Rictor*-ASO in mouse $CD4^+$ T cells. (B) Treatment scheme of *Rictor*-/Ctrl-ASO in MRL/*lpr* mice. (C) Kaplan–Meier cumulative survival plot of *Rictor*-ASO and Ctrl-ASO treated MRL/*lpr* mice. (D) Proteinuria changes of *Rictor*-ASO and Ctrl-ASO treated MRL/*lpr* mice over 28 weeks. Urine (E) and serum (F) creatinine concentration of MRL/*lpr* mice at 19 weeks. (G) Serum urea nitrogen concentration at 19 weeks. (H) Tiers of anti-dsDNA (left) and anti-histone (Right) antibodies in mouse serum at 19 weeks. Serum inflammatory cytokine concentration (I) and Ig isotypes concentration (J) at 19 weeks. (K) Representative H&E staining images of kidneys at 19 weeks; Left: quantitative cortex inflammation grade; right: number of foci. Scale bar: 100 μm. ns, not significant; *$p < 0.05$, **$p < 0.01$. The Kaplan–Meier estimator was used for survival curve analysis (C). Unpaired student t-tests were used for two groups comparison (E – K). Error bars represent SEM.

Figure 5: Anti-human *RICTOR*-ASO reduces antibody production in an *in vitro* T-B cell coculture assay. (A) Immunoblot showing the deletion of RICTOR in human $CD4^+$ T cells. (B) Experiment scheme of the *in vitro* T-B cell coculture assay. (C) Ig isotypes concentration in coculture supernatant after 7 days. (D) Signal intensity heatmap of antibodies against autoantigens in culture supernatant. (E) Paired analysis of autoantibodies signals detected in culture supernatant. ns, not significant; *$p < 0.05$, **$p < 0.01$. p-Values were calculated with paired t-tests. Error bars represent SEM.

Supplementary Methods

Flow cytometry

The following antibodies were used in flow cytometry: anti-B220 (RA3-6B2), anti-CD4 (GK1.5), anti-CD8a (53-6.7), anti-CD25 (PC16), anti-CD38 (90), anti-CD69 (H1.2F3), anti-GL7 (GL-7), anti-CD138 (281-2), anti-IgD (11-26c.2a), anti-CD95 (Jo2), anti-PD-1 (J43), anti-IgM (II/41), and anti-CD162 (2PH1). CXCR5 and PNA were stained with biotinylated anti-CXCR5 (2G8) or biotinylated peanut agglutinin (FL10-71), followed by staining with streptavidin-conjugated PE (BD Biosciences).

SCIENTH method

Cells were rested in complete medium at 37ºC for 30 minutes before equally divided into four parts and seeded into 96 well plates. Wells were treated with vehicle or the following metabolic inhibitors for 15 minutes, 2-Deoxy-D-Glucose (2-DG, 100 mM), Oligomycin (Oligo,1 mM), or a sequential combination of the two. Puromycin (10 µg/ml) was then added to each treated well for 15 minutes. Cells were then washed with ice-cold PBS and stained with Fc receptors and viability dye at RM for 15 minutes. Cells were then stained with surface markers in FACS buffer at RM for 20 minutes. Following washing, cells were fixed and permeabilized using the FOXP3 fixation and permeabilization kit (Biolegend) following the manufacturer's instructions. Cells were next stained with anti-Puromycin AF647 (Sigma Aldrich, clone 12D10), resuspended in FACS buffer and read on an Attune NxT (ThermoFisher) cytometer.

T-B coculture assay

628 CD4+ T cells were first enriched from the healthy or SLE donor PMBC using an enrichment kit
629 (STEMCELL, Cat# 17952). The B220-CD3+CD4+CXCR5+PD-1+CXCR3- cells were sorted as
630 Tfh-like cells. Tfh cells (3×104 cells/well) were cultured with anti-human RICTOR- or Ctrl-ASO
631 (10 nm), IL2 (100 U/ml), and IL7 (10 ng/ml) for 5 days. CD19+ B cells were next enriched from
632 same donor PBMC using an enrichment kit (STEMCELL, Cat# 17854). CD19+IgD-CD27+
633 CD38- cells were next sorted as memory B cells (2×104 cells/well) and seeded to coculture with
634 ASO treated Tfh cells in the presence of staphylococcal enterotoxin B (SEB, 100ng/ml, Toxin
635 Technology) for 7 days.

636 **Supplementary Table 1. Demographic and clinical characteristics of SLE patients***

Patient	**1**	**2**	**3**	**4**	**5**
Age (years)	57	36	55	67	53
Gender	Female	Male	Female	Female	Female
Race/Ethnicity	White non-Hispanic	White non-Hispanic	White non-Hispanic	White non-Hispanic	White non-Hispanic
SLE duration (Years)	28	12	7	12	19
SLEDAI 2k Score	9	10	10	4	0
Autoantibodies					
ANA	+	+	+	+	+
Anti-Sm	-	+	-	+	-
Anti-RNP	+	-	-	+	-
Anti-Ro	+	-	-	-	-
Anti-La	+	-	-	-	-
Anti-dsDNA	+	+	-	-	-
aCL IgM / IgG	-	Not available	Not available	+/+	-
β2GP1 I IgM / IgG	-	Not available	Not available	-	-
Lupus anticoagulant	-	Not available	Not available	-	+
Complement C3/4	Low	Normal	Normal	Normal	Normal
Organ Involvement					
Joints	+	+	+	+	+
Constitutional	-	-	-	-	-
Hematologic	+	-	-	-	+
Mucocutaneous	-	+	+	-	+
Kidney	-	-	-	-	-
Serosal	+	-	-	-	-
Neuropsychiatric	-	-	-	-	-
Treatments					
Glucocorticoids	+	+	-	+	-
HCQ	+	-	+	+	+
Mycophenolate	-	-	-	-	-
Methotrexate	-	-	+	+	-
Azathioprine	-	-	-	+	+
Others	None	None	None	None	None

637

638 *All patients met ACR/EULAR SLE criteria.

639 Abbreviations: ANA=antinuclear antibodies; dsDNA=anti-double-stranded DNA antibody;
640 RNP=anti-Ribonucleoprotein antibody. Sm=anti-Smith antibody; Ro=anti-Ro antibody; La=anti-
641 La antibody; SCL70= anti-topoisomerase I; RF= Rheumatoid Factor. ACCP= Anti-cyclic
642 citrullinated peptide, aCL = anticardiolipin; anti-β2GPI = anti–β2-glycoprotein I, HCQ=
643 Hydroxychloroquine.
644

Supplementary figure legend

Supplementary Figure 1: Flow analysis of splenocyte cell populations in IMQ mice.

(A) Expression of GL7 and IgD in splenocyte. Right, frequency of $GL7^{-}IgD^{+}$ naïve B cells. (B) Expression of CD21 and CD23 in splenocyte. Right, frequency of $CD21^{+}CD23^{-}$ marginal zone B cells. (C) Expression of Bcl6 and B220 in splenocyte. Right, frequency of $B220^{+}Bcl6^{+}$ cells. (D) Expression of CD11c and B220 in splenocyte. Right, frequency of $CD11c^{+}B220^{+}$ cells. (E) Expression of Foxp3 and CD4 in splenocyte. Right, frequency of $Foxp3^{+}$ cells within $CD4^{+}$ cells. (F) Expression of T-bet and CD4 in splenocyte. Right, frequency of $CD4^{+}T\text{-}bet^{+}$ cells within $CD4^{+}$ cells. (G) Expression of Ly6C and B220 in splenocyte. Right, frequency of $B220^{+}Ly6C^{+}$ pDC cells. (H) Expression of CD11c and CD11b in splenocyte. Right, frequency of $CD11c^{+}$ $CD11b^{+}$ cDC cells. (I) Expression of Ly6C and CD11b in splenocyte. Right, frequency of $CD11b^{+}Ly6C^{+}$ monocytes. (J) Expression of Ly6G and CD11b in splenocyte. Right, frequency of $CD11b^{+}Ly6G^{+}$ neutrophils. $*p < 0.05$, $**p < 0.01$, $***p < 0.001$. p-Values were calculated with unpaired student t-tests. Error bars represent SEM.

Supplementary Figure 2: Flow analysis of peripheral lymphocytes in Lpr-*Ifnar1*$^{-/-}$ **mice.**

(A) Expression of CD69 and CD4 in pLN derived lymphocytes. Left, frequency of $CD4^{+}CD69^{+}$ population; right absolute cell number of $CD4^{+}CD69^{+}$ cells in pLN. (B) Expression of B220 and CD4 in pLN derived lymphocytes. Left, frequency of $CD4^{+}B220^{-}$ population; right absolute cell number of $CD4^{+}B220^{-}$ cells in pLN. (C) Expression of B220 and CD138 in pLN derived lymphocytes. Left, frequency of $B220^{+}CD138^{hi}$ population; right absolute cell number of $B220^{+}CD138^{hi}$ cells in pLN. (D) Expression of B220 and Bcl6 in pLN derived lymphocytes. Right, frequency of $B220^{+}Bcl6^{+}$ population in pLN. (E) Expression of ICOS on $CD4^{+}$ cells in pLN. (F)

668 Expression of Foxp3 and CD4 in pLN derived lymphocytes. Left, frequency of $CD4^+Foxp3^+$
669 population; right absolute cell number of $CD4^+Foxp3^+$ cells in pLN. (G) Expression of CXCR5
670 and Bcl6 in pLN derived lymphocytes. Upper left, frequency of $CXCR5^+Bcl6^+$ population; upper
671 right, absolute cell number of $CXCR5^+Bcl6^+$ cells in pLN. Lower left, frequency of $CXCR5^+Bcl6^-$
672 population; lower right, absolute cell number of $CXCR5^+Bcl6^-$ cells in pLN. Results were pooled
673 from at least 3 independent experiments. ns, not significant; *p < 0.05, **p < 0.01, ***p < 0.001,
674 ****p < 0.0001. p-Values were calculated with one-way ANOVA with the post-hoc Tukey test.
675 Error bars represent SEM.
676
677 **Supplementary Figure 3: Flow analysis of peripheral lymphocytes in Ctrl-/*RICTOR*-ASO**
678 **treated MRL/*lpr* mice.** (A) Peripheral lymph node size (left) and derived lymphocyte cell
679 numbers (Right) in treated mice. (B) Expression of CD4 and CD8 in pLN derived lymphocytes.
680 Right, percentage of $CD4^+$ population in pLN. (C) Expression of CD4 and CD69 in pLN derived
681 lymphocytes. Right, frequency of $CD4^+CD69^+$ population in pLN. *p < 0.05, **p < 0.01. p-Values
682 were calculated with unpaired student t-tests. Error bars represent SEM.
683
684 **Supplementary Figure 4: Supernatant immunoglobulin isotypes concentration of T-B culture**
685 **derived from healthy donor PBMCs.** ns, not significant, *p < 0.05, **p < 0.01. p-Values were
686 calculated with paired t-tests. Error bars represent SEM.

Figure 1

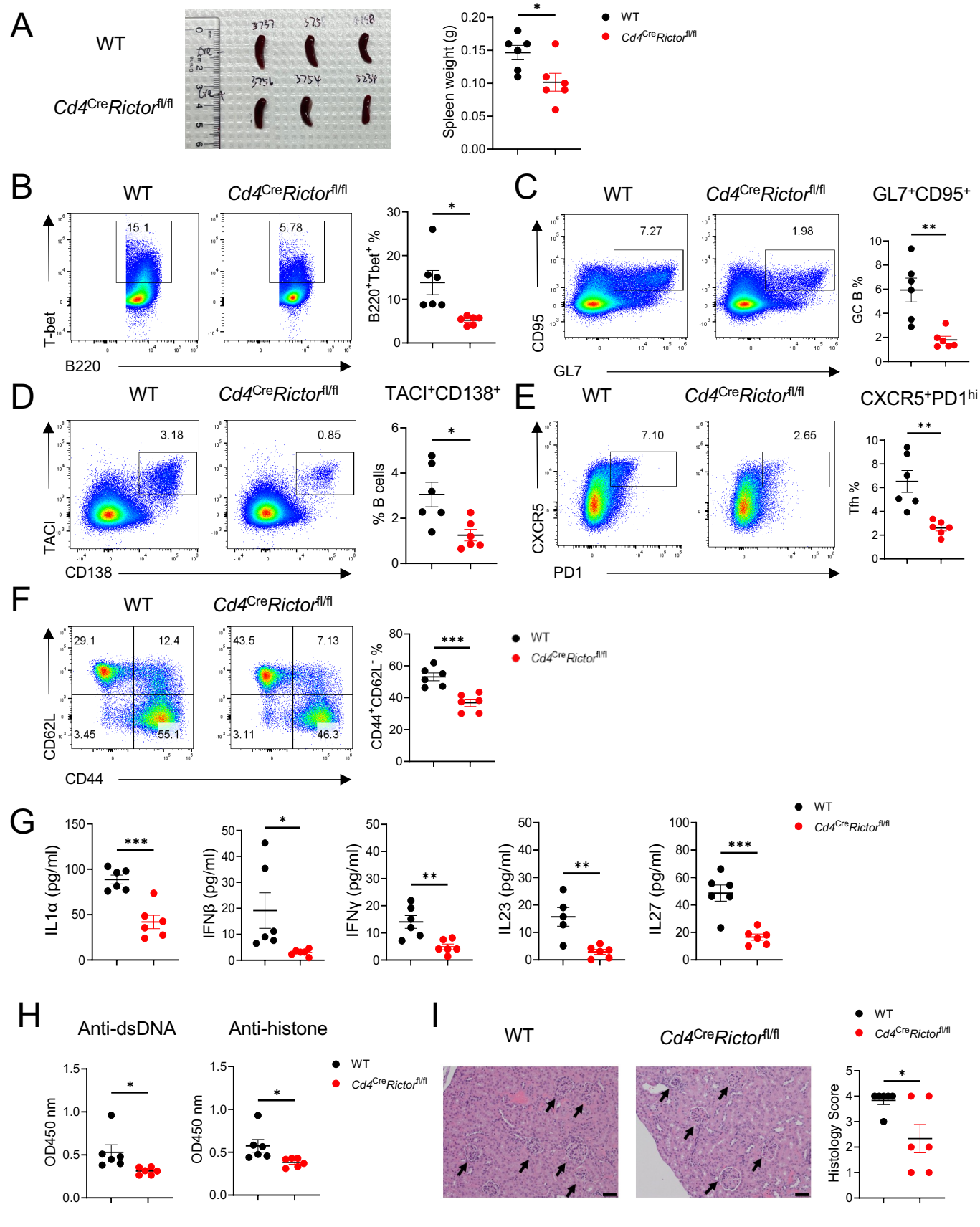

Figure 2

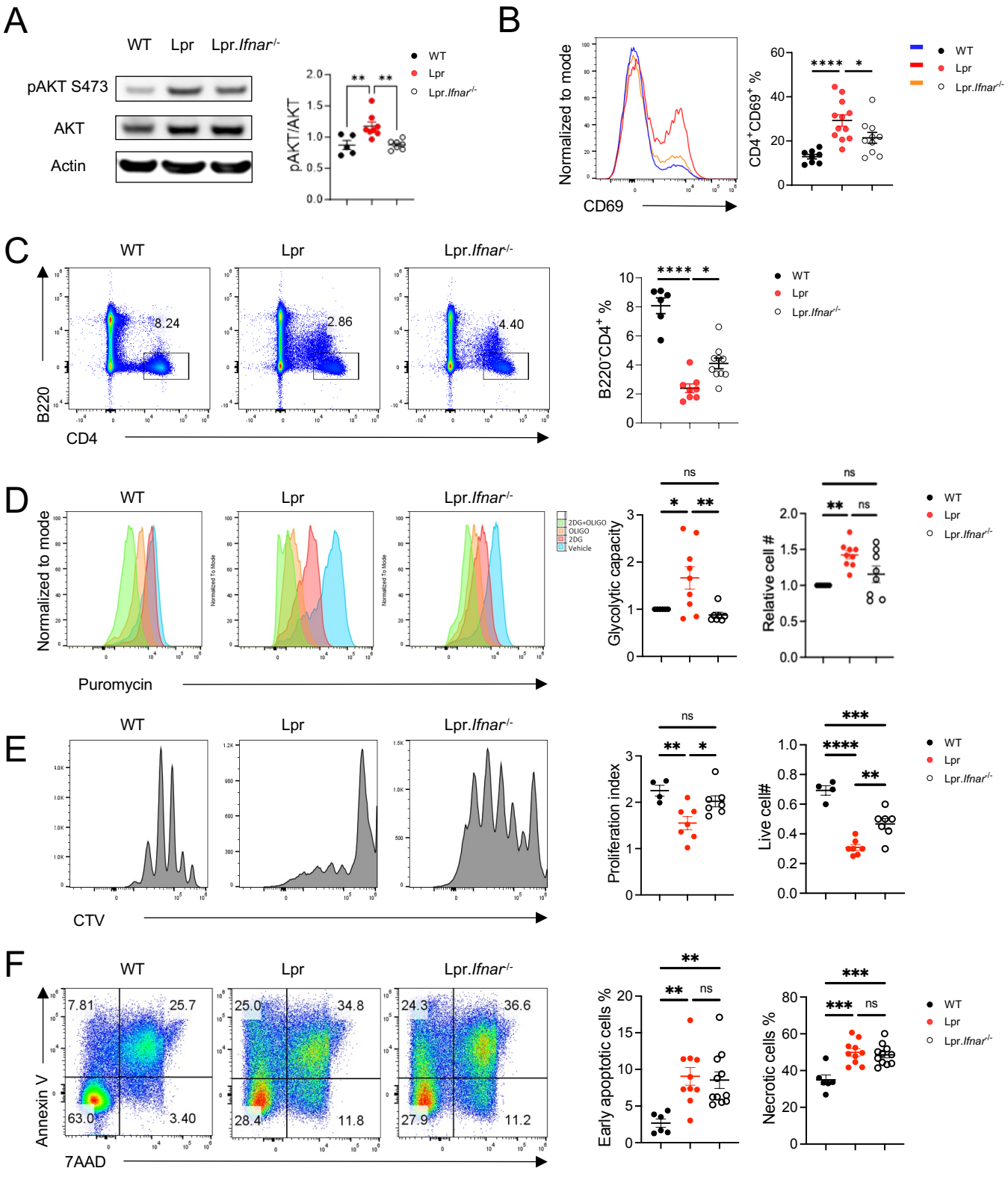

Figure 3

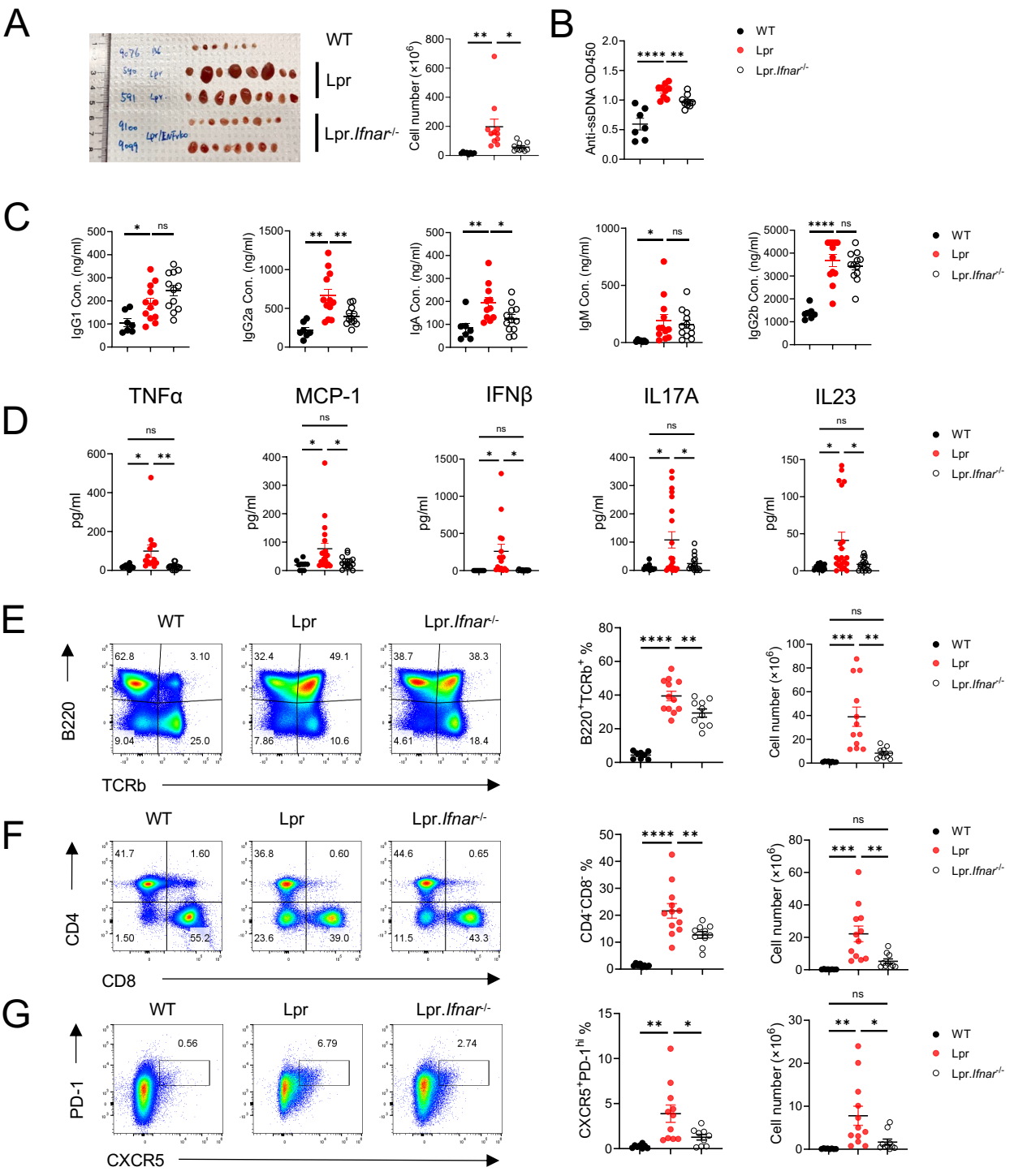

Figure 4

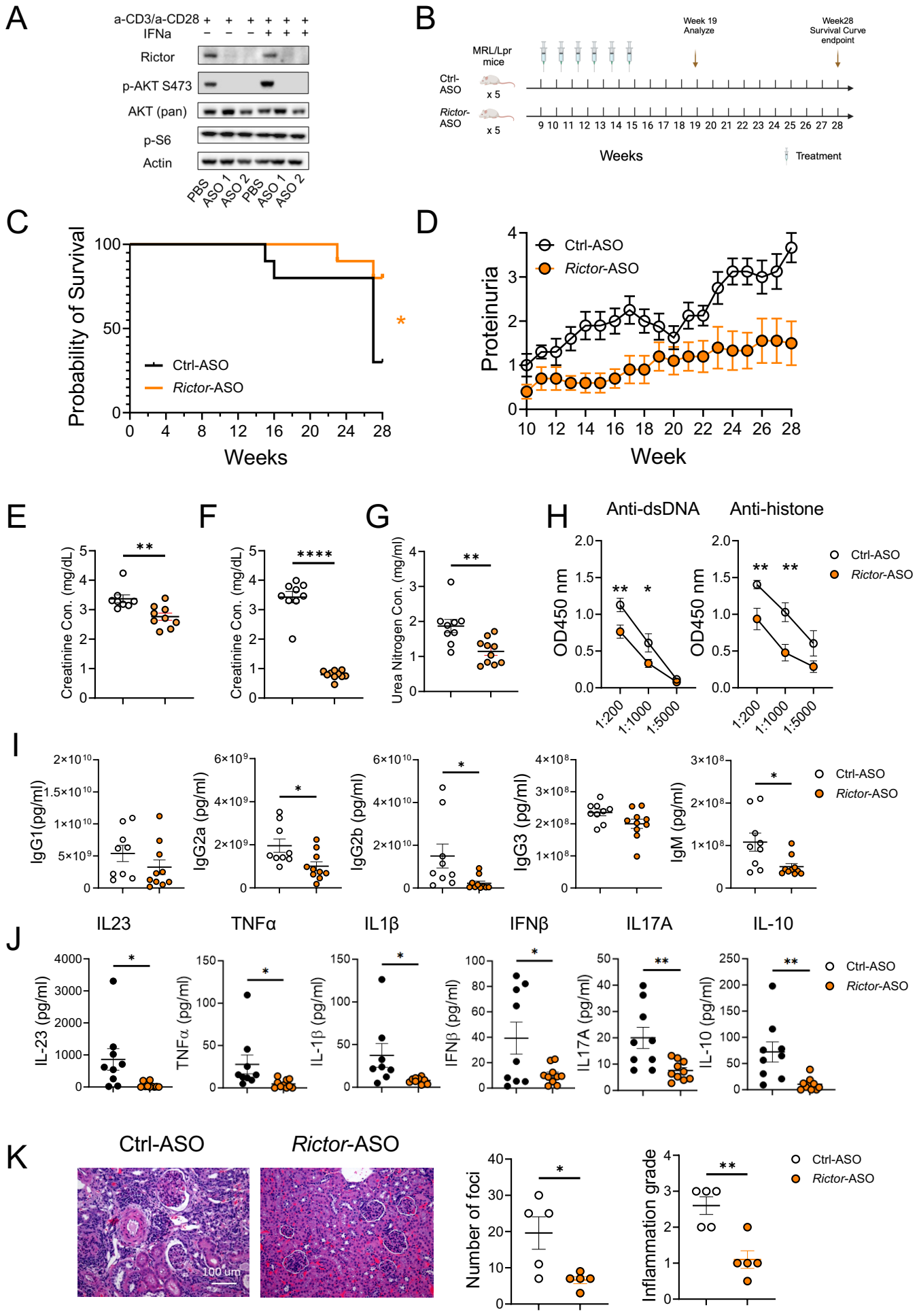

Figure 5

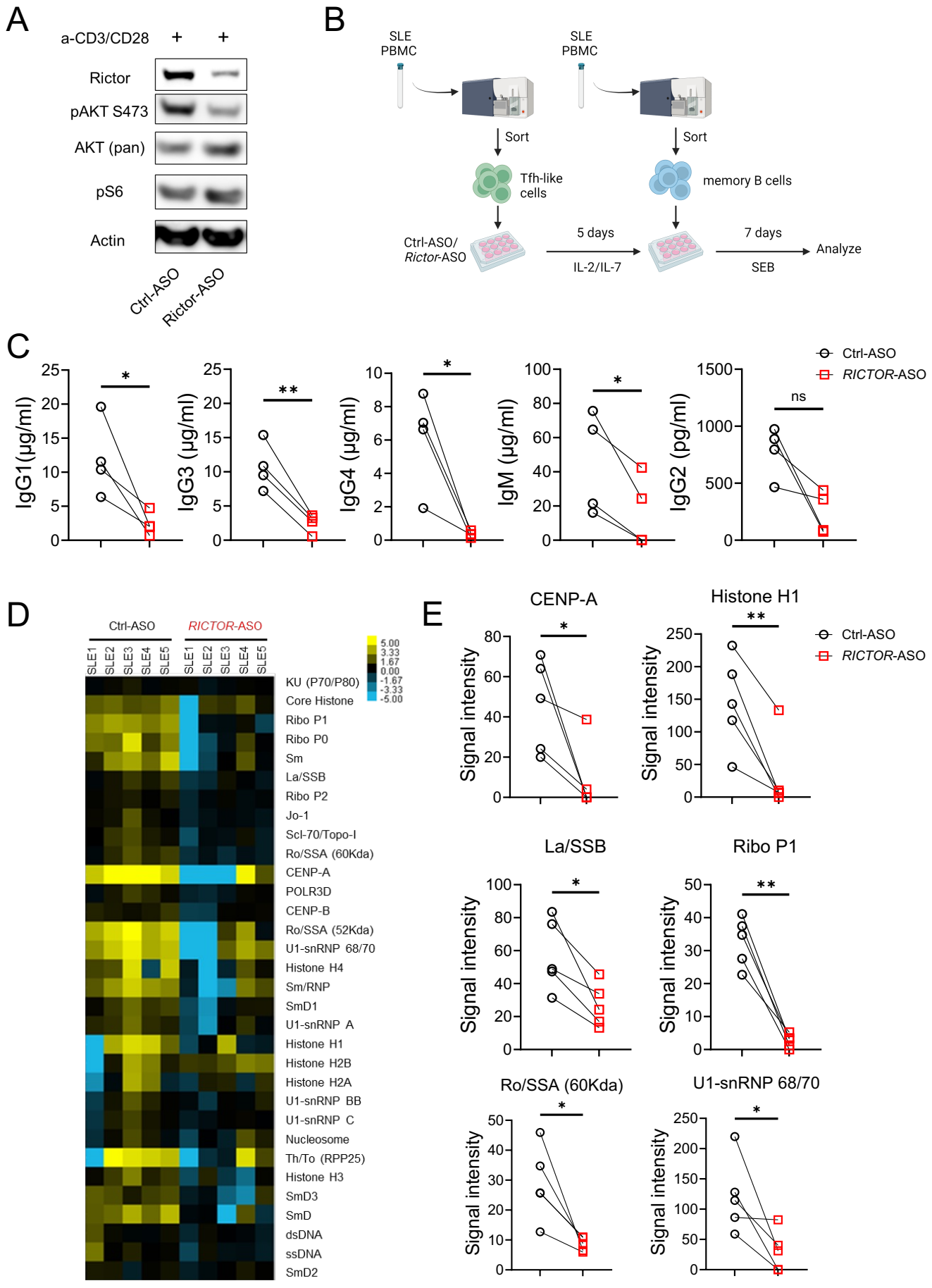

Supplementary Figure 1

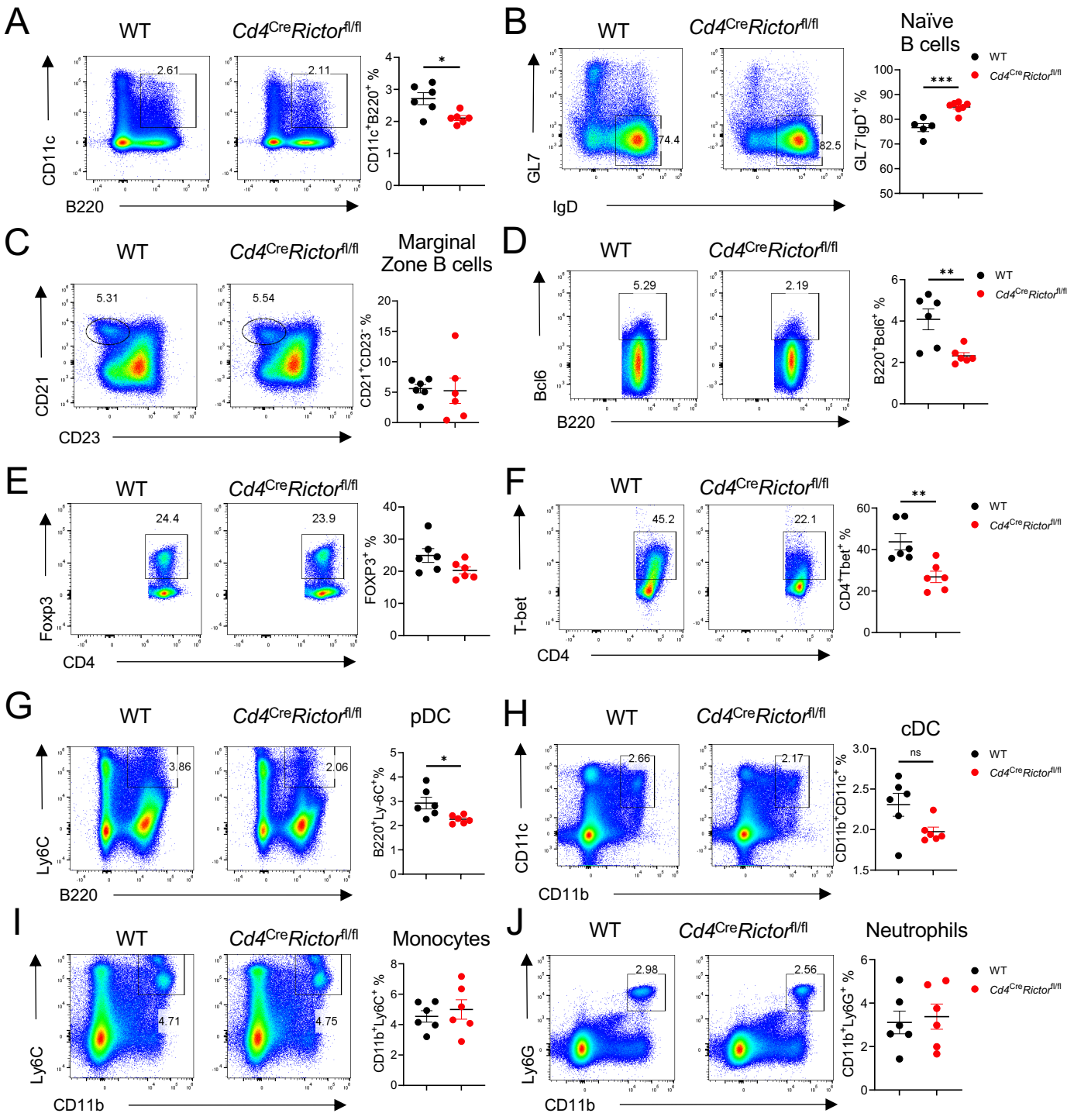

Supplementary Figure 2

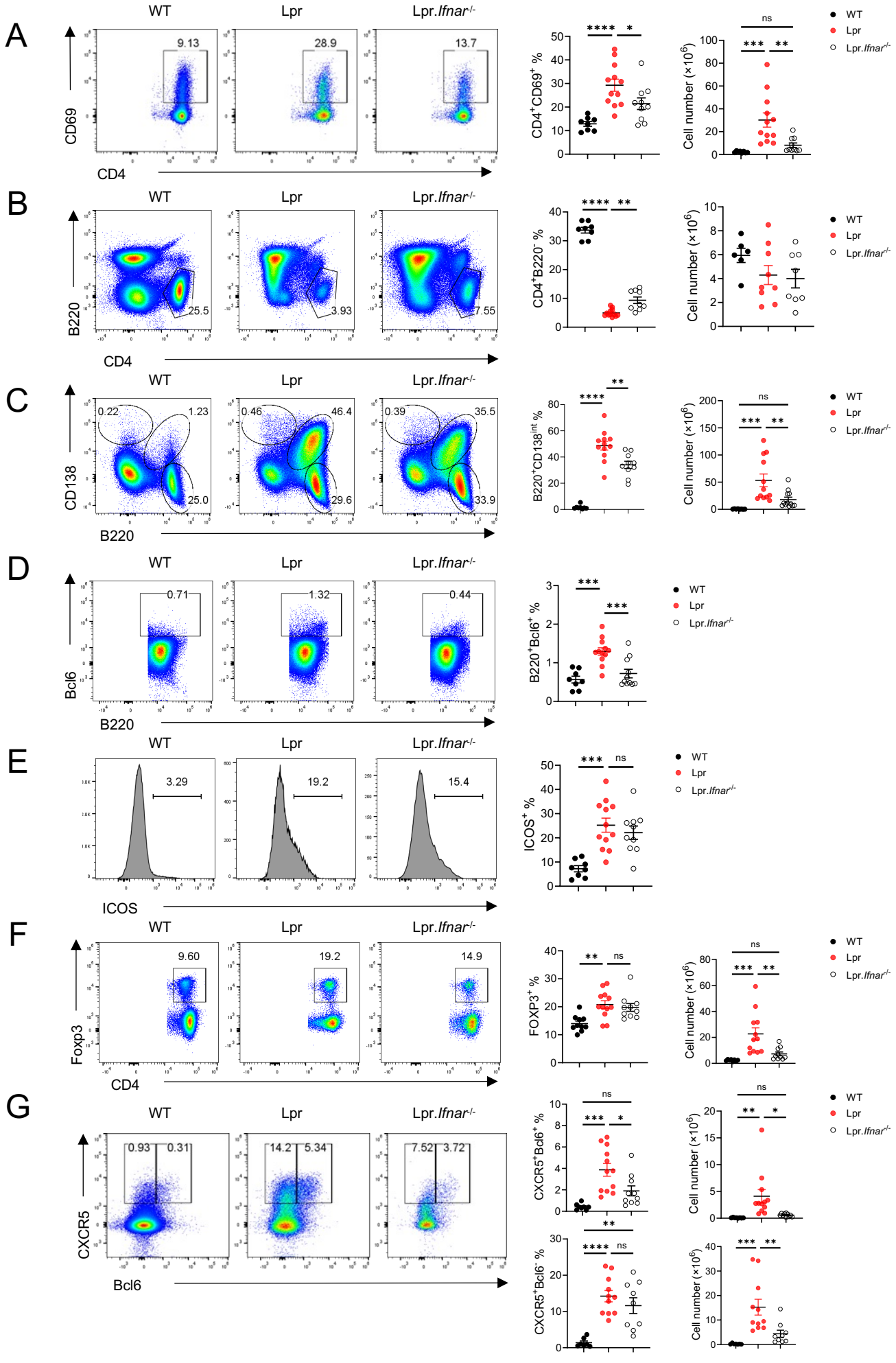

Supplementary Figure 3

Supplementary Figure 4